

Epitaxially strained SnTiO₃ at finite temperatures

D. Wang,^{1,*} L. Liu,^{2,†} J. Liu,³ N. Zhang,⁴ and X. Wei⁴

¹*School of Microelectronics and State Key Laboratory for Mechanical Behaviour of Materials, Xi'an Jiaotong University, Xi'an 710049, China*

²*College of Materials Science and Engineering, Guilin University of Technology, Guilin, 541004, China*

³*State Key Laboratory for Mechanical Behavior of Materials,*

School of Materials Science and Engineering, Xi'an Jiaotong University, Xi'an, China, 710049

⁴*Electronic Materials Research Laboratory-Key Laboratory of the Ministry of Education and International Centre for Dielectric Research, Xi'an Jiaotong University, Xi'an 710049, China*

Combining effective Hamiltonian and direct *ab initio* computation, we obtain the phase diagram of SnTiO₃ with respect to epitaxial strain and temperature, demonstrating the complex features of the phase diagram and providing insight into the epitaxially strained SnTiO₃, a presumably simple perovskite. In the phase diagram, two triple points are found, which may be exploited to achieve high-performance piezoelectric effects. On the other hand, despite the inclusion of the degree of freedoms related to oxygen octahedron tilting, it is found that ferroelectric displacements dominate the structural phases over the whole strain misfit range. Finally, it is shown that the SnTiO₃ can be converted from hard to soft ferroelectrics with epitaxial strain.

I. INTRODUCTION

Piezoelectricity is a phenomenon in certain materials that strain and electric polarisation can induce and/or influence each other. Ferroelectric materials, which are inherently piezoelectric, can produce an electric polarisation proportional to the load, in response to an applied mechanical strain. Similarly, such materials will produce a mechanical deformation (strain) in response to an applied voltage. Switchable polarisation makes ferroelectrics a critical component in memories, actuators, electro-optic devices, and potential candidates for nanoelectronics¹.

In recent years, it has been found that materials of high-performance piezoelectricity are often associated with morphotropic boundary (MPB), with examples including Pb(Zr,Ti)O₃² and (K,Na)NbO₃-LiTaO₃-LiSbO₃³, or triple points, e.g. in (Ba,Ca)(Zr,Ti)O₃⁴. Such phase boundaries and tricritical points are created by engineering solid solutions to a certain composition, where the crystal structure changes abruptly and the piezoelectric properties are maximal. There are three important situations that have been extensively studied: (i) MPB in pure perovskites that separates regions of tetragonal from rhombohedral symmetry⁵; (ii) MPB formed in perovskites dissolved with a small amount of non-perovskite-structured materials that can cause lattice distortions³ and grain boundary effects⁶; (iii) Regions close to a triple point where cubic paraelectric phase (C), ferroelectric rhombohedral (R), and tetragonal (T) phases meet⁴. In addition, another important method to engineer desired ferroelectric materials is epitaxial thin-film growth and the introduction of intrinsic lattice strain. Epitaxial films are of great importance for highly integrated design and intelligent control technology^{7,8}. Strain engineering has been widely adopted to tune the large *2p-3d* charge hybridisation between the strongly correlated *3d* electrons in transition metal ions and *2p* electrons of oxygens⁹⁻¹². For instance, both compressive and tensile strains increase the Ni *3d* band width and favour the metallic phase in NdNiO₃¹³. In addition, substrate clamping will force the temperature dependence of in-plane lattice parameters of films to follow that of the substrates, which may

lead to unexpected phase transitions and domain formation in epitaxial films¹⁴. Therefore, strain constraint as an attractive method to fine tuning properties of films, can even introduce multi-phase coexistence in thin films.

Nowadays commonly used high-performance piezoelectric materials, including PbTiO₃ and Pb(Mn,Nb)O₃, contain hazardous lead (Pb). Since Pb is harmful to environment and human health, lead-free ferroelectric materials are highly desired. Many lead-free materials are based on (Bi_{0.5},Na_{0.5})TiO₃, (K,Na)NbO₃ or BaTiO₃, however, their performance is still sub-optimal compared to Pb-containing materials¹⁵. Since Sn and Pb belong to the same family, SnTiO₃ is expected to achieve high-performance piezoelectricity with environmentally benign elements¹⁶. Indeed, it has been shown that SnTiO₃ has large polarisation and large axial ratio^{17,18}, even larger than PbTiO₃, which makes it a promising candidate. But for various reasons, SnTiO₃ bulk material was still unavailable so far, mainly due to the fact that Sn²⁺ is easy to become Sn⁴⁺, and Sn is prone to enter into the B site (where the Ti ion stays) due to its small ionic radius. However, researchers continued to look for opportunities of exploiting the remarkable properties of SnTiO₃. For instance, Xie *et al* considered Sn-doped BaTiO₃¹⁹, Bennett *et al* considered Sn(Al_{0.5},Nb_{0.5})O₃²⁰, while Suzuki *et al* obtained Sn-doped SrTiO₃²¹, and Laurita investigated (Sr,Sn)TiO₃ and (Ba,Ca,Sn)TiO₃²².

In addition to experimental work, there are also many theoretical investigations on SnTiO₃^{16,18,23-27}. However, most of previous theoretical investigations are based on direct *ab initio* computation, which cannot provide information regarding SnTiO₃ at finite temperatures. Therefore, important questions remain unanswered. For instance, what are the conditions for the existence of different ferroelectric phases? How is the phase diagram of SnTiO₃ like? Can such a seemingly simple perovskite (SnTiO₃ is not solid solution and no doping is applied) possess complex features? In this work, we will focus on the finite temperature properties of epitaxially strained SnTiO₃ and address these questions. We note that such information will be useful for the fabrication of SnTiO₃ bulk, or the growth of SnTiO₃ film, and engineering SnTiO₃-containing ferroelectric materials. Since SnTiO₃ bulk is not

available, there is not much *a priori* information that can be used in this work. While our computational results are less convincing without support from experiments, it demonstrates the value of theoretical and numerical work, i.e., the power to predict something new – this is one of the reasons that motivated us to carry out this investigation.

II. METHOD

To fully understand SnTiO_3 , it is desired to know all the its possible phases under various conditions. However, achieving such a goal is trivial. For instance, the direct *ab initio* approach usually provides us with the structural phase of local energy minimum (in contrast to the most stable phase of global energy minimum), which is exacerbated by the 0 K assumption usually adopted in such computations. The application of this approach will involve the comparison of many different phases, which are often not guaranteed to be complete. To address this problem, here we adopt the first-principles based effective Hamiltonian approach and Monte-Carlo (MC) simulations, which were developed exactly to address such challenges. To use this approach, the price to pay is the need to compute tens of coefficients appearing the effective Hamiltonian using direct *ab initio* computation before carrying out the MC simulations.

We employ the effective Hamiltonian approach combined with Monte-Carlo simulation to obtain finite temperature properties SnTiO_3 . The effective Hamiltonian used here was originally developed in Ref.²⁸, which incorporates the coupled dynamics of the soft mode, strain, and dipole interactions. Its internal energy is given by

$$E = E^{\text{FE}}(\{\mathbf{u}_i\}, \{\mathbf{v}_i\}, \eta_H),$$

where \mathbf{u}_i is the local soft-mode in unit cell i , and is proportional to the local electric dipole moment in that cell, when multiplied by Born effective charge. We note that \mathbf{u}_i here is located on the A-site (where Sn stays), and represents the collective motion of Sn, Ti, and O atoms inside one unit cell. The \mathbf{v}_i are Sn-centered local displacements related to the inhomogeneous strain inside each unit cell. η_H is the homogeneous strain tensor. The energy terms and associated parameters can be found in Ref.²⁹. In this work, we extended the effective Hamiltonian and expanded the local energy term to 8th order (similar to Ref.³⁰) in order to describe the internal energy more precisely³¹. In addition, the antiferro-distortive (AFD) oxygen octahedron tilting is also considered with the energy term being³²

$$E = E^{\text{AFD}}(\{\omega_i\}, \{\mathbf{u}_i\}, \{\mathbf{v}_i\}, \eta_H),$$

where the new variable ω_i represents the oxygen tilting in unit cell i , and centres on the B-site atom (i.e., Ti). The energy term E^{AFD} also includes the couplings between AFD, and all the other dynamical variables. The associated parameters in E^{AFD} are obtained in a similarly way as in Ref.^{29,33}. The effective Hamiltonian approach is a well established methodology that has been developed since 1994^{28?} and, Similar to

DFT, it has been used in many investigations, e.g., to predict new structural phases of perovskites^{35,36}. We note the most appealing features of this approach are (i) it can often lead us to the structural phase of global energy minimum; (ii) it can obtain finite temperature properties, which also explains why we need this approach in this work.

With the effective Hamiltonian, we perform Monte-Carlo simulation on a $12 \times 12 \times 12$ supercell, containing 8640 atoms. The system is set to meet the periodic boundary condition along the (pseudo) x, y, z direction and subject to various epitaxial strain. In each simulation at a given epitaxial misfit strain s , we gradually cool down the system from 2500 K down to 5 K. For each temperature, we carry out 160,000 Monte Carlo steps to obtain averaged physical quantities, most importantly, the supercell average of local mode, which can be used to determine the symmetry of the system and the approximate positions of each atom in it.

We have also performed direct *ab initio* computation to corroborate first-principles-based Monte-Carlo simulation results. For this purpose, the open source ABINIT software package cite³⁷ is used along with the local density approximation (LDA)³⁸ and the projector-augmented-wave (PAW) method³⁹. We use the pseudo-potentials implemented in the GBRV package⁴⁰, and the Sn $4d\ 5s\ 5p$, Ti $3s\ 3p\ 4s\ 3d$, and O $2s\ 2p$ orbitals are treated as valence orbitals. For convergence, we have chosen the cut-off energy (`ecut`) to be 25 Hartree (1 Hartree = 27.211 eV) for plane wave expansion, and fine grid of the cut-off energy (`pawcutdg`) is selected to be ~ 50 Hartree in all calculations. In addition, k -point sampling of $6 \times 6 \times 6$ Monkhorst-Pack grid⁴¹ was used. The atomic coordinates are relaxed until all atomic-force components are smaller than 10^{-5} Ha/Bohr, and the cell size and shape are varied until all stress components are below 10^{-7} Hartree/Bohr³.

Before showing the simulation results, it is worth mentioning that, comparing to our previous work²⁹, the present investigation develops in three directions: (i) We now include the new degree of freedom, i.e., oxygen octahedron tilting (often called antiferrodistortive rotations, AFD), which is ignored in the previous work²⁹. (ii) To this end, we computed many new essential parameters for the effective Hamiltonian. While the current work build on the previous one, it has substantially extended the effort to fully simulate SnTiO_3 . (iii) Here we consider the effects of epitaxial strain. and show that SnTiO_3 has a rather complex phase diagram. containing interesting phase boundaries and triple points.

III. RESULTS

In order to obtain the phase diagram, we have performed MC simulations for misfit strain between $s = 0$ and $s = 2\%$ with a step size of $\Delta s = 0.125\%$. For each misfit strain s , the system is gradually cooled down from ~ 2500 K to 5 K and observe the evolution of the system with temperature. The simulation results are then summarized to form the phase diagram.

A. Phase transition and phase diagram

We first obtain the supercell averaged local mode versus temperature of SnTiO_3 under various tensile epitaxial strains, which is expected to be able to stabilise SnTiO_3 ¹⁸. Such information enables us to find the evolution of structural phases with respect to temperature and epitaxial strain, and more importantly, the phase transition temperatures of the system. Figure 1 shows the results with epitaxial strain $s = 0.375\%$ and $s = 1\%$. Note that we have relaxed the cubic phase ($Pm\bar{3}m$) SnTiO_3 using ABINIT (with settings specified in Sec. II) to obtain the lattice parameter $a = 7.312$ Bohr, which is used as the reference value for specifying the misfit strain.

For the smaller epitaxial strain $s = 0.375\%$, the system adopts $P4mm$ phase for temperature $T \lesssim 1000$ K, ($P_x = P_y = 0, P_z > 0$), as temperature increases it undergoes a phase transition to become the $Amm2$ phase ($P_x = P_y > 0, P_z = 0$), and eventually adopts the cubic phase for $T \gtrsim 1500$ K. The whole process is a little similar to that of BaTiO_3 and $(\text{Na}_{0.5}\text{K}_{0.5})\text{NbO}_3$, where several structural phases are involved in phase transitions. Here, however, a rather drastic change happens at around 1000 K as the polarisation rotates from out-of-plane to the in-plane configuration. For the larger epitaxial strain ($s = 1\%$), there are also two phase transitions. At low temperature ($T \lesssim 197$ K), it adopts the Cm ($P_x = P_y > 0, P_z > 0$) phase, which changes to the $Amm2$ phase as the temperature increases, and finally become paraelectric at $T \simeq 1750$ K. This phase transition temperature is high comparing to other typical ferroelectric materials, e.g., PbTiO_3 (763 K) and BiFeO_3 (1100 K). The reason is likely due to the strong dipole-dipole interaction inside SnTiO_3 , noting that the spontaneous polarization of SnTiO_3 (1.32 C/m^2)²⁹ is larger even larger than strained BiFeO_3 (1.30 C/m^2)⁴².

It is worth noting that no correlated AFD tilting of oxygen octahedron was observed for the epitaxial strains investigated here, which are consistent with previous known results¹⁸ (also see Sec. IV). Figure 1 indicates that four phases (paraelectric $Pm\bar{3}m$, orthorhombic $Amm2$, tetragonal $P4mm$, and monoclinic Cm) phase can all exist in SnTiO_3 at proper temperature and epitaxial strain. Consistent with previous results²⁹, without strain constraint or at very small strain ($s < 0.5\%$, see Fig. 2), the system adopts the $P4mm$ phase ($P_z > 0, P_{x,y} = 0$) at low temperature, and only has one phase transition ($P4mm$ to paraelectric) as temperature increases. Interestingly, Figure 1(b) shows a region ($T \leq 200$ K) that corresponds to the M_B phase (belong to space group Cm)^{31,43}, and for smaller s (e.g., at $s = 0.75\%$), we have observed that $P_z > P_x = P_y$, which is also Cm , but corresponds to the M_A phase⁴³. Moreover, in Figure 1(a), both M_A and M_B phases exist between the T ($P4mm$) and O ($Amm2$) phases. The phase transition sequence is similar to the local structure evolution of $\text{Pb}(\text{Ti}_{1-x}, \text{Zr}_x)\text{O}_3$ with increasing x ⁴⁴. We note that such monoclinic region has been shown to play critical role in high-performance piezoelectric materials⁴⁵.

We now turn to the phase diagram of SnTiO_3 with respect to temperature and epitaxial strain. To this end, we performed simulations similar to that of Fig. 1 at different epitaxial

strains and obtained the results shown in Fig. 2, which demonstrates several important features. First, for all the investigated strain misfit (up to 2%), Fig. 2 shows that SnTiO_3 undergoes a paraelectric to ferroelectric phase transition at rather high temperature ($T_C > 1400$ K). The reason for the high T_C is likely due to the large intrinsic spontaneous polarisation, which was discussed in a previous work²⁹. Second, T_C initially decreases with s , reaching a minimum, and then increases again⁴⁶, the lowest point corresponds to a triple point separating the paraelectric phase and the other two ferroelectric phases (tetragonal $P4mm$ and orthorhombic $Amm2$), similar to what happens in ultrathin PbTiO_3 films⁴⁷. Our simulation show that the abrupt transition from the $P4mm$ to the Cm phase (with respect to the misfit strain) happens in a very narrow region ($< 0.125\%$), which is represented by a straight line in Fig. 2 due to the limit of Δs used in simulations.

We note that the first triple point in Fig. 2, where one paraelectric cubic phase and two ferroelectric phases converge, is a good place to look for giant piezoelectric effects in lead-free materials. For instance, such triple point was found and exploited in binary compounds including $(\text{Ba}_{0.7}, \text{Ca}_{0.3})\text{TiO}_3$ - $\text{Ba}(\text{Zr}_{0.2}, \text{Ti}_{0.8})\text{O}_3$ (BCZT)⁴, $\text{Ba}(\text{Sn}_{0.12}, \text{Ti}_{0.88})\text{O}_3$ - $x(\text{Ba}_{0.7}, \text{Ca}_{0.3})\text{O}_3$ ⁴⁸, and other BaTiO_3 -derived systems⁴⁹. More importantly, a second triple point exists, where three ferroelectric phases ($P4mm$, $Amm2$, and Cm) converge. There are three boundaries around this point. The boundary at $s = 0.5\%$ separates the $P4mm$ and the Cm phase, resembling the MPB seen in $\text{Pb}(\text{Zr}_{1-x}, \text{Ti}_x)\text{O}_3$, in which two different structural phases exist with a buffer region at $x \simeq 0.48$. In $\text{Pb}(\text{Zr}_{1-x}, \text{Ti}_x)\text{O}_3$ the monoclinic phase serves as a bridge between the higher symmetry tetragonal phase (with [001] polarisation) and the rhombohedral phases (with [111] polarisation)³². In this connecting phase, the polarisation has the freedom to align anywhere on the {110} mirror plane between the pseudocubic [111] and [001] directions, giving rise to the high piezoelectric response^{32,50,51}.

Here in SnTiO_3 , the pronounced existence of the Cm phase and the second triple point, which plays a similar role of bridging the tetragonal phase (with [001] polarisation) and the orthorhombic phase (with [110] polarisation), may also enable high performance, following the pattern of the universal phase diagram discussed in Ref.^{50,51}. The reason is similar to that of $\text{Pb}(\text{Zr}_{1-x}, \text{Ti}_x)\text{O}_3$: in this region, polarisation anisotropy nearly vanishes and thus polarisation rotations are easy⁴³. It is also worth noting that many alkaline niobate perovskites show a polymorphic phase transition⁵² between tetragonal phase and orthorhombic phase, similar to what happens in Fig. 2. The polymorphic behaviour can also lead to high piezoelectricity due to the instability with respect to polarisation rotation⁵³. However, the temperature stability of their piezoelectric properties for alkaline niobate perovskites is not as good as $\text{Pb}(\text{Zr}_{1-x}, \text{Ti}_x)\text{O}_3$. In addition, the large anisotropy along the whole polymorphic boundary line leads to a larger energy barrier between the two polarisation states (tetragonal and orthorhombic), preventing possible polarisation rotations because the phase coexistence results from the diffusive tetragonal to orthorhombic phase transformation.⁴ In

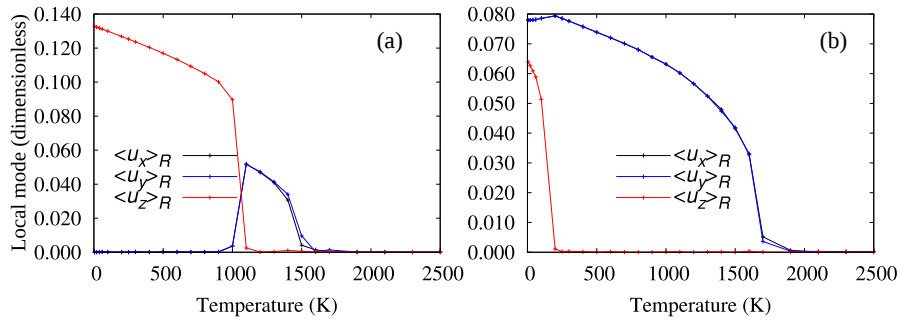


Figure 1. Local mode versus temperature at two given strain misfit, $s = 0.375\%$ (Left panel) and $s = 1\%$ (Right panel).

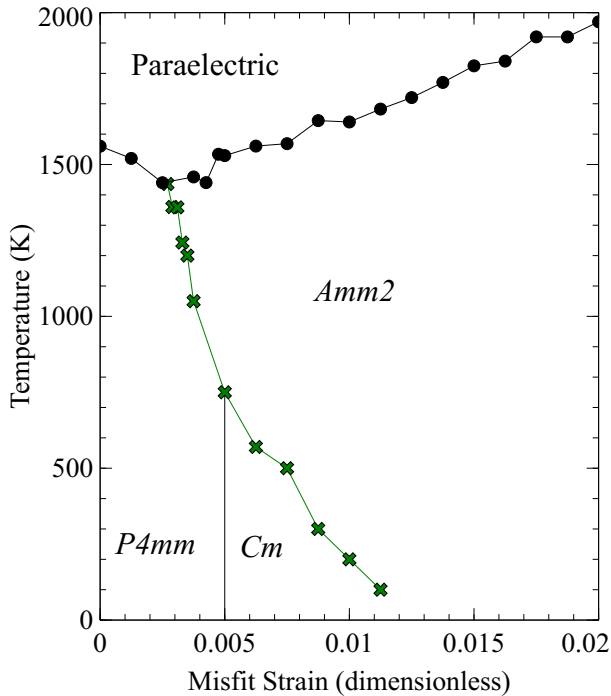


Figure 2. Phase diagram of epitaxially strained SnTiO_3 .

SnTiO_3 , unlike polymorphic phase transition, the Cm phase is associated with a triple point, where a low energy barrier between two ferroelectric phases ($P4mm$ and $Amm2$) may exist that facilitates the polarisation rotation and lattice distortion, leading to high performance. Unfortunately, this triple point is not at room temperature for pure SnTiO_3 (which is at ~ 750 K as shown in Fig. 2), and may need to be tuned (e.g. by doping). For instance, following the lessons from BCZT, it may be possible to use Pb to substitute Sn and/or Zr to substitute Ti. In this way, SnTiO_3 can be taken as the matrix material for designing high performance piezoelectric materials.

To show that the polarisation in the Cm phase is indeed easy to rotate, we also obtained the hysteresis loop at different epitaxial strains. As Fig. 3 shows, the Cm phase has a strong effect on the hysteresis loop of SnTiO_3 . When the Cm phase exists [Fig. 3(a)] at $s = 0.75\%$, the coercive field

is $\sim 1.6 \times 10^7$ V/m, reduced by a factor of 10 compared to the result obtained when $s = 0\%$ ($> 2 \times 10^8$ V/m, see Fig. 3(b)). In analogous to magnetic materials, by applying a proper strain (e.g., 0.75%), SnTiO_3 become “soft” ferroelectrics. Interestingly, in the whole process, the magnitude of the polarisation \mathbf{P} is approximately a constant [dark green line in Fig. 3], making the whole process a rotation as well as switching of polarisation (albeit a sudden rotation), consistent with previous computation^{26,27}.

B. Results from direct *ab initio* computation

To corroborate results obtained from effective-Hamiltonian-based computation, we also obtained numerical results from direct *ab initio* computation. Figure 4(a) shows the energy versus strain for the $P4mm$, $Amm2$, and Cm phases. These phases all appear in the phase diagram of SnTiO_3 (Fig. 2). For a large range of epitaxial strain, the Cm phase has the lowest energy. At $s = 1\%$, the energy of the Cm phase is approximately 29.4 meV lower than that of $P4mm$ or $Amm2$. Such results indicate that the Cm phase can be the ground state for a restricted range of strain, which supports our effective Hamiltonian results. The reason that the Cm phase appears at $s = 0.5\%$ is likely due to the fact that, at this point, the three phases (Cm , $P4mm$, and $Amm2$) have similar energies, and macroscopically the average of $P4mm$ and $Amm2$ also give rise to the Cm phase. On the other hand, when $s > 1\%$, $P4mm$ is no longer an option as its energy becomes much higher than the other two. As the energy difference continue to be smaller with strain, the Cm phase can only exist at low temperature, and eventually disappears. We also note that the Cm phase rarely appear in pure perovskites, whether it is epitaxially strained or not, and SnTiO_3 seems to be an important exception. Figure 4(b) plots the polarisation versus strain for the Cm phase, which is similar to the results obtained in Ref.¹⁸, showing that P_z increases while $P_{x,y}$ decreases with increasing epitaxial strain. We finally note that, despite many attempts, no structural phases involving oxygen octahedron tilting were found to be the ground state. For $0\% < s < 5\%$, structural phases without oxygen octahedron tilting are consistently more stable in terms of energy.

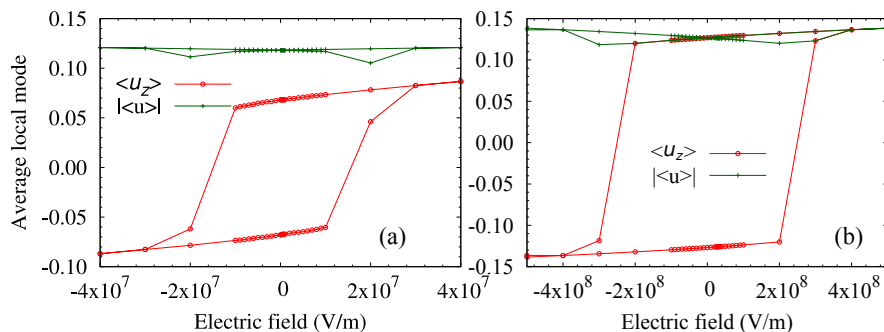


Figure 3. Hysteresis loop of SnTiO₃ at $s = 0.75\%$ (a) and $s = 0\%$ (b) at 300 K. The electric field is applied along the z -axis.

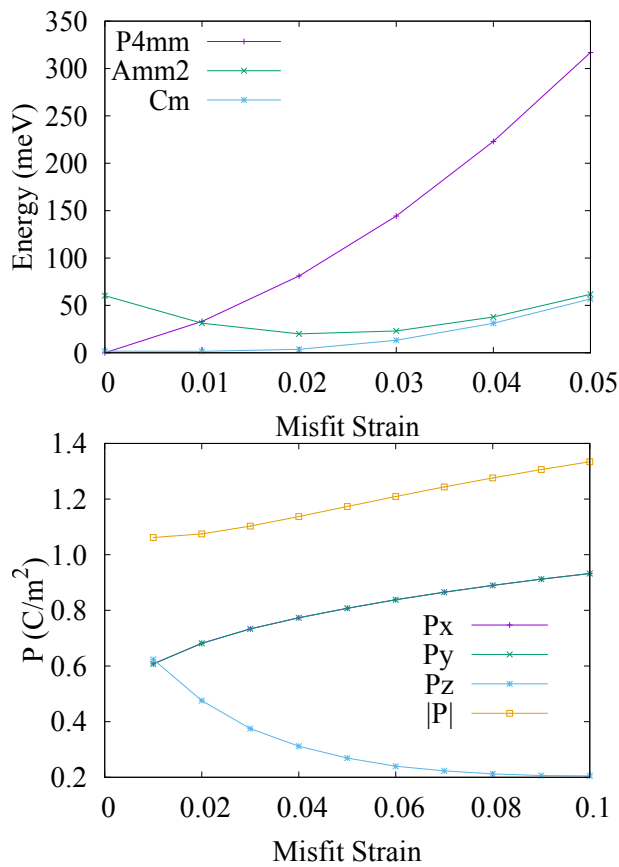


Figure 4. (a) Energy and polarisation versus strain for three different phases $Amm2$, $P4mm$, and Cm . At $s = 0\%$; (b) The polarisation ($P_x = P_y$ and P_z) versus strain for the Cm phase.

IV. DISCUSSION

In Sec. III, we have shown that SnTiO₃ has $P4mm$, $Amm2$ and Cm phases under different conditions. However, it is hard to prove that SnTiO₃ can only have these three phases for the misfit strain we have investigated. This point is further discussed below in Sec. IV A. Moreover, we will compare the MC results to direct *ab initio* results and focus on the Cm phase in Sec. IV B.

A. Seeking new phases

Phonon calculations have shown that for SnTiO₃ the AFD-related modes are also unstable¹⁸. Considering this fact, it is rather surprising that we the MC simulation results are not able to identify new phases involving oxygen octahedron tilting, which is a pity and important lesson.

Moreover, we had intentionally played with the coefficients in the effective Hamiltonian and performed additional MC simulations in order to suggest new phases involving AFD. The simulation results indeed generated a few AFD-related candidates (e.g., the $Ima2$, $Imma$, and $I4cm$ phases). However, direct *ab initio* calculations do not validate as energy ground states, consistent with the fact that Parker et al did not propose any AFD-related phases although their calculation shows strong AFD instability¹⁸. Therefore, our results strongly suggest that SnTiO₃ may not have AFD-related phases as ground state for epitaxial misfit strain of $s < 5\%$.

The reason AFD-related phases do not appear is most likely due to the strong competition from the polar modes, which are responsible for the polarization in SnTiO₃. For ferroelectric materials, AFD is usually an adverse factor to the development of polarization. One term in the effective Hamiltonian specifically represents such an effect, which is $D\omega^2\mathbf{u}^{254}$, where the sign of the coupling coefficient (D) will determine how strong the competition (or in rare cases the cooperation) between the local mode \mathbf{u} (related to polarization) and ω (related to AFD). In SnTiO₃, apparently the ferroelectric modes (which are responsible for the $P4mm$, $Amm2$, and Cm phases) play the most important roles.

B. The Cm phase

The results from *ab initio* computation in Fig. 4 show that the Cm phase has the lowest energy beyond $s = 0$ among the $P4mm$, Cm and $Amm2$ phases. On the other hand, the phase diagram obtained from the effective Hamiltonian shows that SnTiO₃ exhibits the Cm phase in a much smaller misfit strain range. The reason of this discrepancy is that the lone pair on Sn²⁺ can cause the extra out-of-plane polarization that is not well accounted for in the effective Hamiltonian.

In the effective Hamiltonian approach, the polar-

ization is closely related to the Γ -point (of the cubic phase) unstable polar mode Zhong1994. For SnTiO_3 it is $u_{x,y,z} = (\xi_{\text{Sn}}, \xi_{\text{Ti}}, \xi_{\text{O}_{\parallel}}, \xi_{\text{O}_{\perp}}, \xi_{\text{O}_{\perp}}) = (0.534, 0.169, -0.411, -0.508, -0.508)$ (normalized), which approximately represents the ion displacements in SnTiO_3 and specifies how spontaneous polarization develops. However, some anomaly happens for SnTiO_3 as can be seen from the direct *ab initio* computation. For instance, at $s = 1\%$, along z direction the ion displacements are $u'_z = (0.847, 0.352, -0.049, -0.27, -0.27)$ while along the x, y directions, $u'_{x,y} = (0.781, 0.259, -0.150, -0.387, -0.387)$. It is more important to note that u' has a much larger weight on Sn^{2+} , which is not reflected in u . In fact, this is a known issue during the development of the effective Hamiltonian approach as discussed in Ref.³⁴ where it was pointed out that for KNbO_3 and PbTiO_3 there is large difference between the experimental and theoretical local modes. Here, we see that SnTiO_3 has the same problem and the difference between PbTiO_3 and SnTiO_3 is discussed in detail in Ref.⁵⁵. In principle, for SnTiO_3 it is possible to tune the values of u (or adding an extra polar mode) in the effective Hamiltonian to alleviate or fix this problem. But such a move will involve many more cumbersome calculations of coupling coefficients, making the approach more complicated. This issue again shows the

complexity of SnTiO_3 despite its simple composition.

V. CONCLUSION

Using effective Hamiltonian based Monte Carlo simulations, we have investigated epitaxially strained SnTiO_3 , found their structural phases at finite temperatures, and obtained its phase diagram with respect to temperature and strain misfit. The phase diagram of SnTiO_3 turns out to be rather complicated, containing two triple points and boundaries that separate ferroelectric phases. Such special features provide unique opportunities to design novel high-performance ferroelectric materials using SnTiO_3 as the matrix, in which the rarely seen Cm phase can exist. In addition, while phonon calculation had shown that AFD related modes are unstable¹⁸, no AFD-related structural phases were found in our simulations, which is likely due to the strong competition from unstable polar modes.

This work is financially supported by the National Natural Science Foundation of China (NSFC), Grant No. 11574246, 51390472, U1537210, and National Basic Research Program of China, Grant No. 2015CB654903. L.L. acknowledges NSFC Grant No. 11564010 and the Natural Science Foundation of Guangxi (GA139008).

* dawei.wang@mail.xjtu.edu.cn

† 2009011@glut.edu.cn

¹ Xu R J, Liu S, Grinberg I, Karthik J, Damodaran A R, Rappe A M and Martion L W 2015 *Nature Mater.* **14** 79

² Jaffe B, Cook W R and Jaffe H 1971 *Piezoelectric Ceramics* (London: Academic)

³ Saito Y, Takao H, Tani T, Nonoyama T, Takatori K, Homma T, Nagaya T and Nakamura M 2004 *Nature* **432** 84

⁴ Liu W F and Ren X B 2009 *Phys. Rev. Lett.* **103** 257602

⁵ Jaffe B, Roth R S and Marzullo S 1954 *J. Appl. Phys.* **25** 809

⁶ Zeng Y, Bokov A A, Wang D, Xiang F, and Hong W, *Ceram. Inter.* 2018 <https://doi.org/10.1016/j.ceramint.2018.06.152>

⁷ Wessels B W 2007 *Ann. Rev. Mater. Res.* **37** 659

⁸ Ramesh R and Spaldin N A 2007 *Nat. Mater.* **6** 21

⁹ Hwang H Y, Iwasa Y, Kawasaki M, Keimer B, Nagaosa N and Tokura Y 2012 *Nature Mater.* **11** 103

¹⁰ Yamada H, Ogawa Y, Ishii Y, Sato H, Kawasaki M, Akoh H and Tokura Y 2004 *Science* **305** 646

¹¹ Ohtomo A and Hwang H Y 2004 *Nature* **427** 423

¹² Spaldin N A and Fiebig M 2005 *Science* **309** 391

¹³ Wang L, Ju S, You L, Qi Y J, Guo Y W, Ren P, Zhou Y and Wang J L 2015 *Sci. Rep.* **5** 18707

¹⁴ He F Z, Wells B O, Ban Z G, Alpay S P, Grenier S, Shapiro S M, Si W D, Clark A and Xi X X 2004 *Phys. Rev. B* **70** 235405

¹⁵ Wu J, Xiao D and Zhu J 2015 *Chem. Rev.* **115** 2559

¹⁶ Armiento R, Kozinsky B, Fornari M and ceder G 2011 *Phys. Rev. B* **84** 014103; Matar S, Baraille I and Subramanian M 2009 *Chem. Phys.* **355** 43

¹⁷ Lebedev A I 2009 *Phys. Solid State* **51** 362

¹⁸ Parker W D, Rondinelli J M and Nakhmanson S M 2011 *Phys. Rev. B* **84** 245126

¹⁹ Xie Y H, Yin S, Hashimoto T, Kimura H and Sato T 2009 *J. Mater.*

Sci. **44** 4834

²⁰ Bennett J W, Grinberg I, Davies P K and Rappe A M 2011 *Phys. Rev. B* **83** 144112

²¹ Suzuki S, Honda A, Iwaji N, Higai S, Ando A, Takagi H, Kasatani H and Deguchi K 2012 *Phys. Rev. B* **86** 060102

²² Laurita G, Page K, Suzuki S and Seshadri R 2015 *Phys. Rev. B* **92** 214109

²³ Taib M F M, Yaakob M K, Hassan O H and Yahya M Z 2013 *Integr. Ferroelectr.* **142** 119

²⁴ Taib M F M, Yaakob M K, Badrudin F W, Kudin T I T, Hassan O H and Yahya M Z A 2014 *Integr. Ferroelectr.* **459** 134

²⁵ Uratani Y, Shishidou T and Oguchi T 2008 *Jpn. J. Appl. Phys.* **47** 7735

²⁶ Zhang R Z, Wang D W, Li F, Ye H J, Wei X Y and Xu Z 2013 *Appl. Phys. Lett.* **103** 062905

²⁷ Zhang R Z, Wang D W, Zhu X H, Ye H J, Wei X Y and Xu Z 2014 *J. Appl. Phys.* **116** 174101

²⁸ Zhong W, Vanderbilt D and Rabe K M 1994 *Phys. Rev. Lett.* **73** 1861; 1995 *Phys. Rev. B* **52** 6301

²⁹ H J Ye, Wang D W, Jiang Z J, Cheng S and Wei X Y 2016 *Acta Phys. Sin.* **65** 237101

³⁰ Nishimatsu T, Iwamoto M, Kawazoe Y, and Waghmare U V 2010 *Phys. Rev. B* **82** 134106

³¹ Vanderbilt D and Cohen M H 2001, *Phys. Rev. B* **63** 094108

³² Kornev I A, Bellaiche L, Janolin P E, Dkhil B and Suard E 2006 *Phys. Rev. Lett.* **97** 157601

³³ Ye H J, Zhang R Z, Wang D W, Cui Y, Wei J, Wang C L, Xu Z, Qu S B and Wei X Y 2013 *Int. J. Mod. Phys. B* **27** 1350144

³⁴ King-Smith R D and Vanderbilt D 1994 *Phys. Rev. B* **49** 5828

³⁵ Jiang Z J, Xu B, Li F, Wang D, and Jia C.-L. 2015 *Phys. Rev. B* **91** 014105

³⁶ Al-Barakaty A, Prosandeev S, Wang D, Dkhil B, Bellaiche L 2015

- Phys. Rev. B* **91** 214117
- ³⁷ Gonze X, Beuken J M, Caracas R, Detraux F, Fuchs M, Rignanese G M, Sindic L, Verstraete M, Zerah G, Jollet F, Torrent M, Roy A, Mikami M, Ghosez P, Raty J Y and Allan D C 2002 *Comp. Mat. Sci.* **25** 478
- ³⁸ Perdew J P and Wang Y 1992 *Phys. Rev. B* **45** 13244
- ³⁹ Blöchl P E 1994 *Phys. Rev. B* **50** 17953
- ⁴⁰ Garrity K F, Bennett J W, Rabe K M and Vanderbilt D 2014 *Comput. Mater. Sci.* **81** 446
- ⁴¹ Monkhorst H J and Pack J D 1976 *Phys. Rev. B* **13** 5188
- ⁴² Zhang J X, et al, 2011 *Phys. Rev. Lett.* **107** 147602
- ⁴³ Zhang N, Yokota H, Glazer A M, Ren Z, Keen D A, Keeble D S, Thomas P A and Ye Z G 2014 *Nat. Commun.* **5** 5231
- ⁴⁴ Lu X, Zheng L, Li H and Cao W 2015 *J. Appl. Phys.* **117** 134101
- ⁴⁵ Liu H, Chen J, Fan L, Ren Y, Pan Z, Lalitha K. V., Rödel J and Xing X, 2017 *Phys. Rev. Lett.* **119**, 017601
- ⁴⁶ Schlom D G, Chen L Q, Eom C B, Rabe K M, Streiffer S K and Triscone J M 2007 *Annu. Rev. Mater. Res.* **37** 589
- ⁴⁷ Jiang Z J, Zhang R Z, Wang D W, Sichuga D, Jia C L and Bel-laiche L 2014 *Phys. Rev. B* **89** 214113
- ⁴⁸ Xue D Z, Zhou Y M, Bao H X, Gao J H, Zhou C and Ren X B 2011 *Appl. Phys. Lett.* **99** 122901
- ⁴⁹ Liu L J, Zheng S Y, Huang Y M, Shi D P, Wu S S, Fang L, Hu C Z and Elouadi B 2012 *J. Phys. D: Appl. Phys.* **45** 295403
- ⁵⁰ Guo R, Cross L E, Park S E, Noheda B, Cox D E and Shirane G 2000 *Phys. Rev. Lett.* **84** 5423
- ⁵¹ Cox D E, Noheda B, Shirane G, Uesu Y, Fujishiro K and Yamada Y 2001 *Appl. Phys. Lett.* **79** 400
- ⁵² Liu L J, Huang Y M, Li Y H, Fang L, Dammak H, Fan H Q and Thi M P 2012 *Mater. Lett.* **68** 300
- ⁵³ Wada S, Suzuki S, Noma T, Suzuki T, Osada M, Kakihana M, Park S E, Cross L E and Shrout T R 1999 *Jpn. J. Appl. Phys.* **38** 5505
- ⁵⁴ Wang D W, et al, 2011 *Phys. Rev. Lett.* **107** 175502
- ⁵⁵ Pitike K C, Parker W D, Louis L, and Nakhmanson S M, 2015 *Phys. Rev. B* **91** 035112